Supplement for:

Structure/Function Analysis of the Human Diabetes Risk Factor and Zinc Transporter ZnT8 (SLC30A8)

Mark J. Daniels [†,‡,*], *Maciej Jagielnicki* [†,‡], *and Mark Yeager* [†,§,||,*]

[†] Department of Molecular Physiology and Biological Physics

University of Virginia School of Medicine

Charlottesville, VA 22908 USA

[§] Department of Medicine

Division of Cardiovascular Medicine

University of Virginia Health System

Charlottesville, VA 22908 USA

[||] Center for Membrane and Cell Physiology

University of Virginia School of Medicine

Charlottesville, VA 22908 USA

* Corresponding author: email -- markjd@virginia.edu

* Corresponding author: email -- yeager@virginia.edu

Table S1. Detergents screened for membrane solubilization and extraction of ZnT8B.

Well	Abbreviation	Name	Vendor	Type	MW	CMC (%)	final %
B4	FC-12	fos-choline 12	Anatrace	zwitterionic	351.5	0.047	0.5
D1	TX-100	Triton X-100	Anatrace	nonionic	647	0.010	4.0
G7	DM	n-decyl-β-D-maltopyranoside	Anatrace	nonionic	482.6	0.087	1.0
G12	DDM	n-dodecyl-β-D-maltopyranoside	Anatrace	nonionic	510.6	0.0087	0.5

Table S2. Detergents screened for ZnT8B solubility.

Well	Abbreviation	Name	Vendor	Type	MW	CMC (%)	final %	DFA	SEC
A4	ZC-14	Anzergent 3-14	Anatrace	zwitterionic	363	0.007	0.021	+	-
A12	CF-6	Cyclofos-6	Anatrace	zwitterionic	349	0.094	0.188	+	-
B4	FC-12 *	fos-choline 12	Anatrace	zwitterionic	352	0.047	0.094	+	+
C12	APB035	Anapoe 35	Anatrace	nonionic	1198	0.011	0.028	+	-
D1	TX-100	Triton X-100	Anatrace	nonionic	647	0.010	0.040	-	-
D2	APX305 **	Anapoe X305	Anatrace	nonionic	1526	0.099	0.248	+	+
E2	APO109	Anapoe C10E9	Anatrace	nonionic	555	0.072	0.18	+	-
E6	APO138	Anapoe C13E8	Anatrace	nonionic	553	0.0055	0.0138	+	-
G2	CYMAL-7	CYMAL-7	Anatrace	nonionic	523	0.01	0.03	+	-
G7	DM	n-decyl-β-D-maltopyranoside	Anatrace	nonionic	483	0.087	0.174	-	-
G9	UDM	n-undecyl-β-D-maltopyranoside	Anatrace	nonionic	497	0.029	0.087	+	-
G12	DDM	n-dodecyl-β-D-maltopyranoside	Anatrace	nonionic	511	0.0087	0.026	-	-
H5	UDTM	n-undecyl-β-D-thiomaltopyranoside	Anatrace	nonionic	513	0.011	0.033	+	-
H7	FA-231	Façade-EM	Avanti	nonionic	1115	0.02	0.040	+	-
H9	DMNG	decyl maltose neopentyl glycol	Anatrace	nonionic	950	0.0034	0.0068	+	-
H10	LMNG	lauryl maltose neopentyl glycol	Anatrace	nonionic	1005	0.001	0.002	-	-
	TFA-1	Façade-TFA1	Avanti	nonionic	2148	0.0028	0.0056	n/d	-

Well coordinates as shown in Figure S3A.

* Best detergent selected based on DFA screen and IMAC/SEC screening

**Detergent promoted high protein solubility, not used for purification due to its chain length

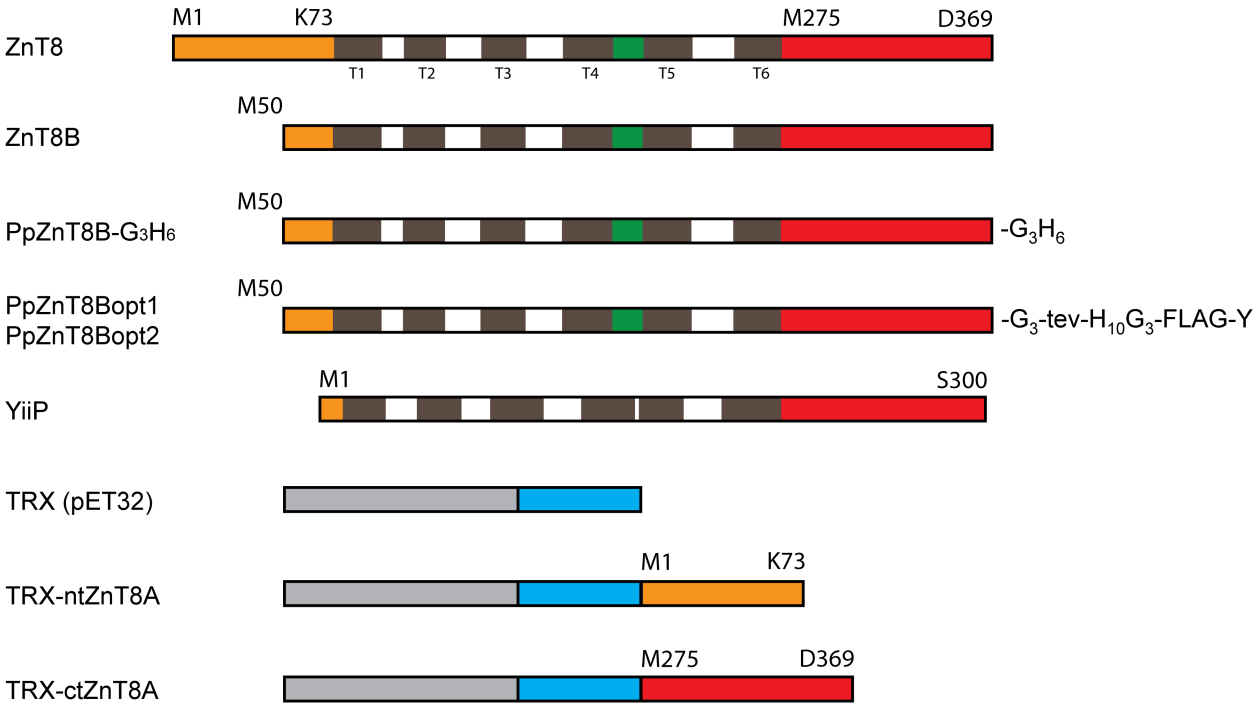

Figure S1. Illustration of protein constructs used in this study. Cytoplasmic amino-terminal domains (orange), cytoplasmic carboxy-terminal domains (red), His-rich loop (green), transmembrane domains of ZnT8 (dark grey), *E. coli* thioredoxin (light grey), linker H_6, thrombin, S*Tag, and enterokinase sequences as encoded by the pET32 vector (blue). Amino acid residue and position above construct shows amino acid residue and position of start or end of domain. Amino acid sequences for PpZnT8Bopt1 and PpZnT8Bopt2 are identical, first construct is codon-optimized using a global *P. pastoris* codon bias, whereas the second is codon-optimized using a *P. pastoris* membrane protein codon bias. FLAG sequence: DYKDDDK, tev sequence: ENLYFQS. Illustration of YiiP shown at bottom for comparison.

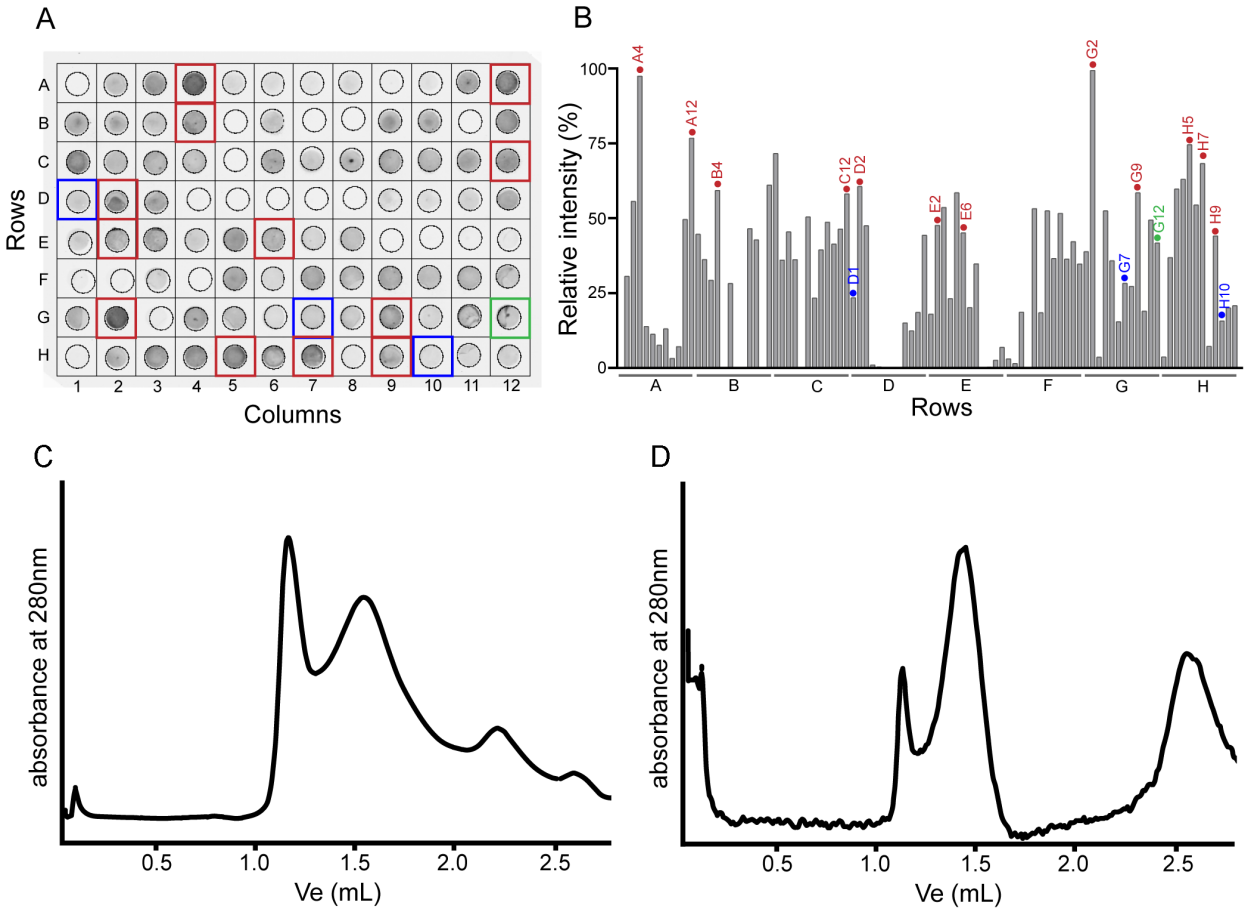

Figure S2. Differential filtration assay (DFA) used to guide detergent selection for protein solubilization. (A) Image of ZnT8 immunoblot showing minimally aggregated, detergent-solubilized protein able to pass through a nitrocellulose membrane with a 300 kDa molecular weight cutoff. (B) Densitometry of immunoblot shown in A. Detergents selected for further analysis by IMAC and SEC were chosen based upon DFA performance (red), success in solubilizing the bacterial homolog YiiP (green), or previous experience in our laboratory (blue). For SEC analysis, proteins were concentrated, then injected onto a Superdex 200 5/150 column and separated by HPLC. Example elution profiles of purified ZnT8B exchanged into FC-12 (C) or APX305 (D) are shown. Well detergents are as described in the Selector Kit method (Anatrace); e.g. FC-12 is B4, APX305 is D1.

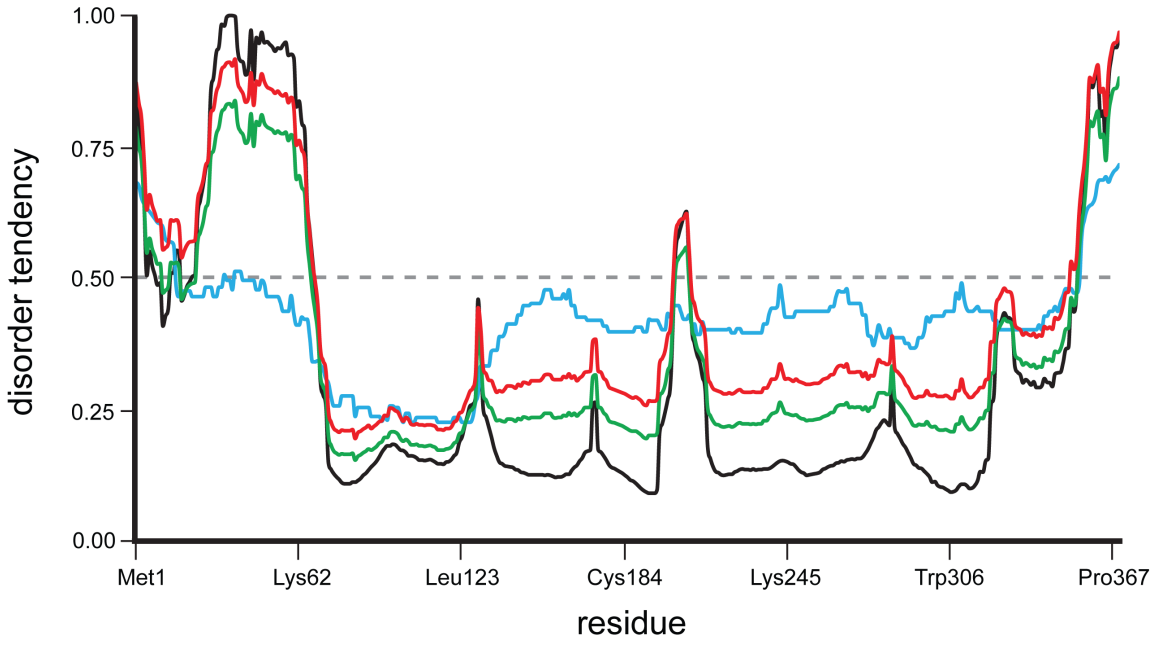

Figure S3. Predictions of disordered residues in ZnT8A. Plot shows disorder index values corresponding to the protein amino acid residues. MetaDisorder [54] consensus shown in black, with results from the 3D method in blue, MD method in green, and MD2 method in red. Residues with a score greater than 0.5 (dashed grey line) are predicted as likely to be disordered.

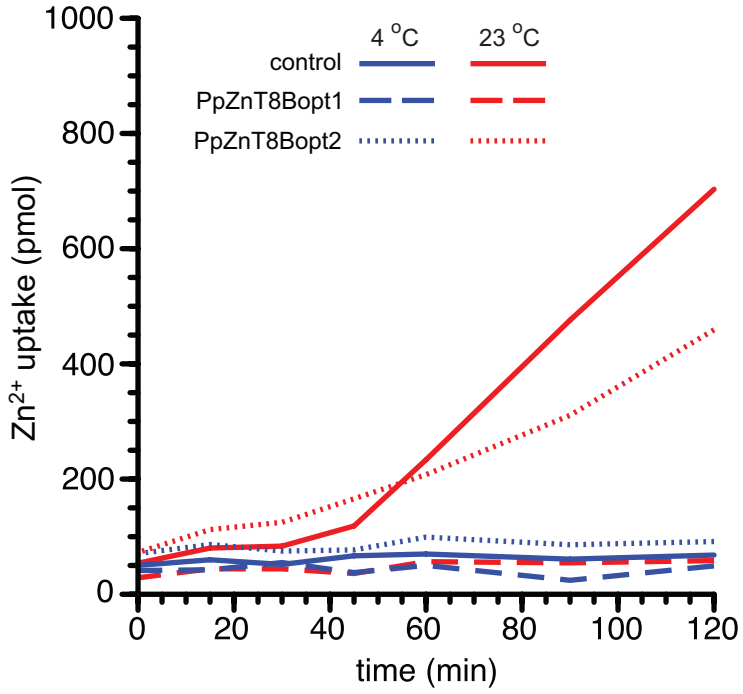

Figure S4. Temperature-dependent $^{65}Zn^{2+}$ uptake indicates that activity is protein-dependent. Yeast overexpressing PpZnT8Bopt1 (dashed line), PpZnT8Bopt2 (dotted line), or expression vector alone (solid line) were incubated at either 23 (red) or 0 ºC (blue), the extracellular media was supplemented with 10 μM $^{65}ZnCl_2$, and aliquots were taken at time points thereafter. Uptake of $^{65}Zn^{2+}$ into the cells was measured using a scintillation counter.

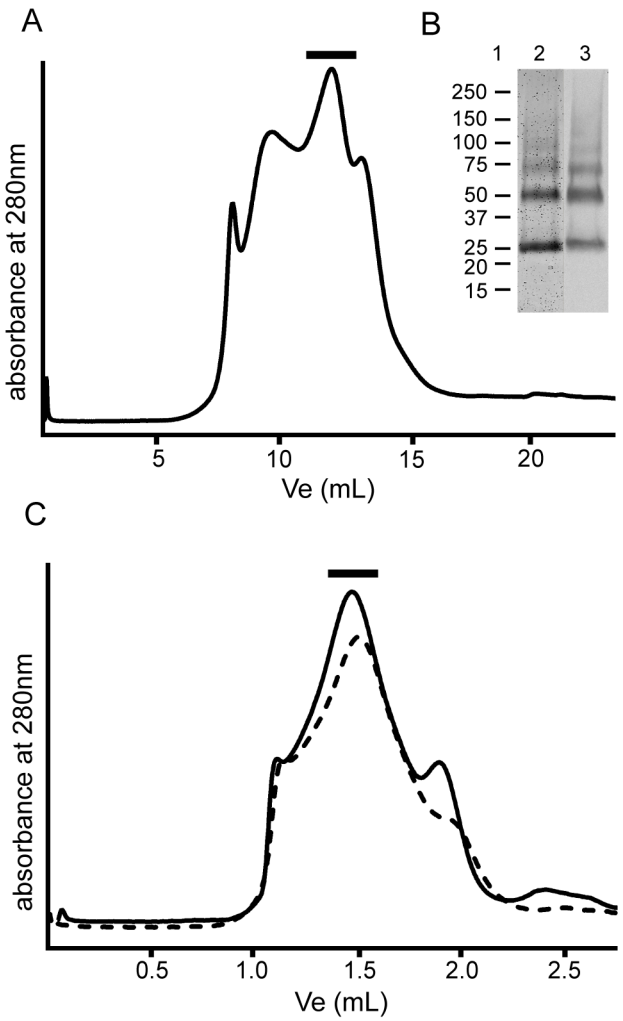

Figure S5. SEC purification of ZnT8B expressed in *P. pastoris*. (A) Peak fractions in the elution profile of apparent mass ~150 kDa indicated (black bar). Inset (B) shows molecular weight markers in kDa (lane 1), Coomassie-stained SDS-PAGE gel (lane 2) and ZnT8 immunoblot (lane 3) of SEC eluate. (C) Elution profile of purified ZnT8B from A incubated at 4 ºC for 5 d (dashed line) or 10 d (solid line), with peak fractions of protein dimer indicated (black bar).

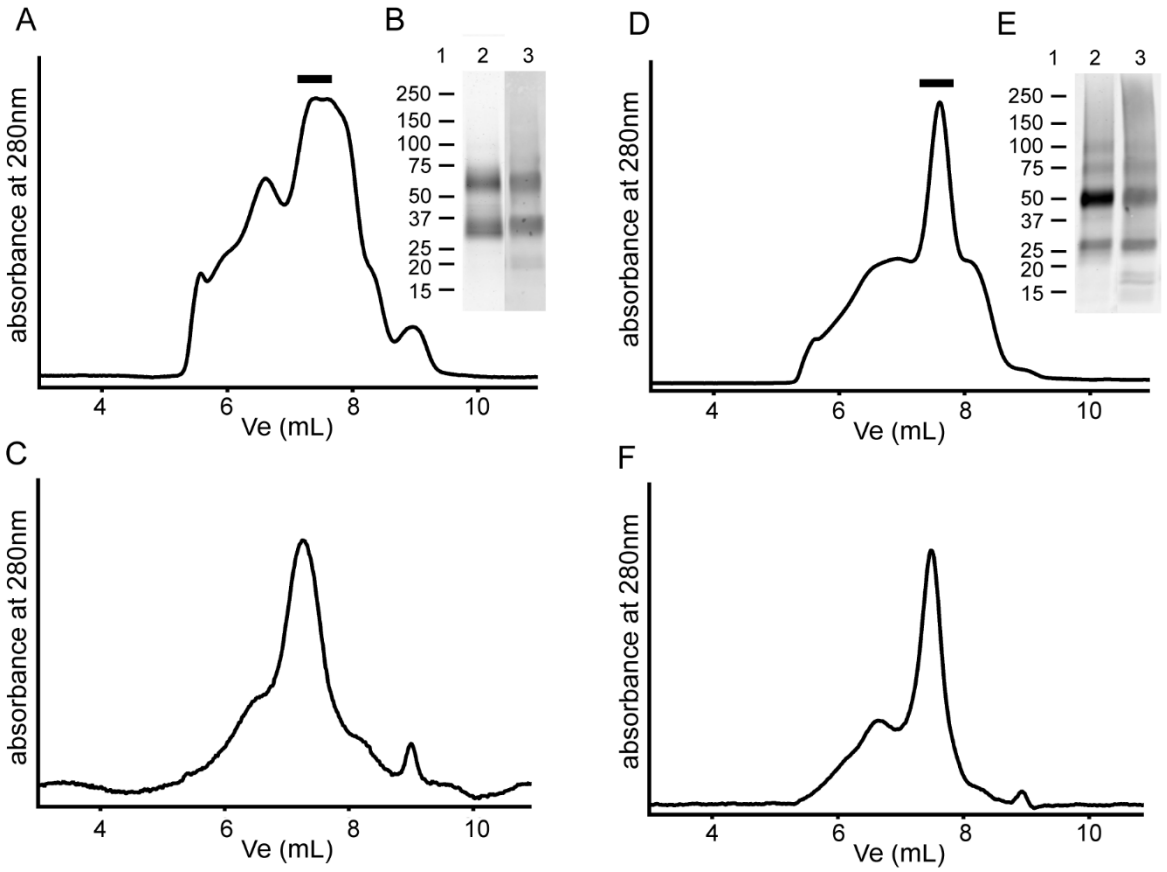

Figure S6. SEC purification of ZnT8 constructs expressed in *S. frugiperda* (Sf9). Peak fractions in the elution profiles of apparent mass ~150 kDa indicated (black bars) for ZnT8A and and ZnT8B shown in (A) and (D), respectively. Insets (B) and (E) for ZnT8A and ZnT8B, respectively, show molecular weight markers in kDa (lane 1), Coomassie-stained SDS-PAGE gel (lane 2) and ZnT8 immunoblot (lane 3) of SEC eluates. Elution profiles of purified ZnT8A from A and ZnT8B from D shown in (C) and (F), respectively, following incubation at 4 ºC for 7 d.

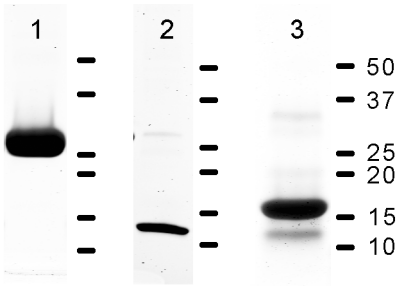

Figure S7. SDS-PAGE of purified proteins used in CD studies. Lane 1, TRX-ntZnT8A; lane 2, ctZnT8A; lane 3, enterokinase-digested bacterial thioredoxin (TRX*). Proteins were stained with SimplyBlue colloidal Coomassie dye. Position of molecular weight markers in kDa shown on the right. Calculated molecular weight of TRX-ntZnT8A is 25.6 kDa, of ctZnT8A is 10.5 kDa, and of TRX* is 17.1 kDa.

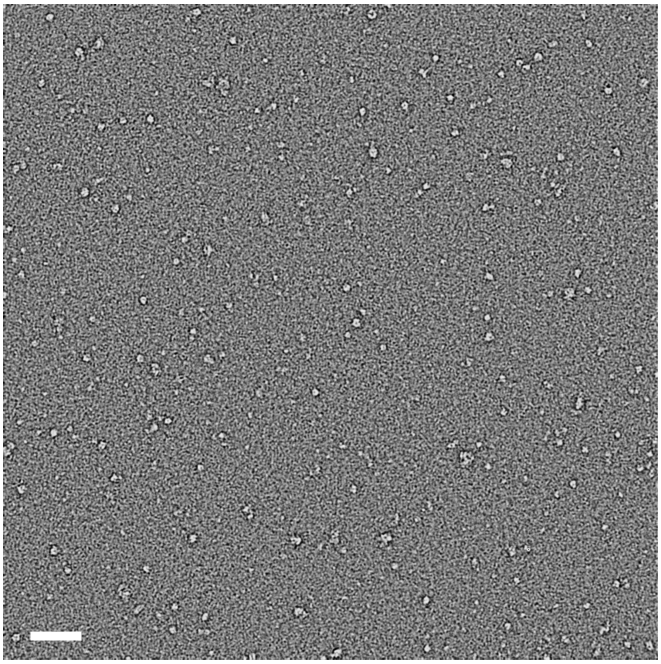

Figure S8. Electron micrograph of purified ZnT8. Particles stained with uranyl formate. The contrast of the micrograph was enhanced by high- and low-pass Gaussian filtering at 100 and 15 Å, respectively. Magnification = 62,000x. Scale bar denotes 50 nm.

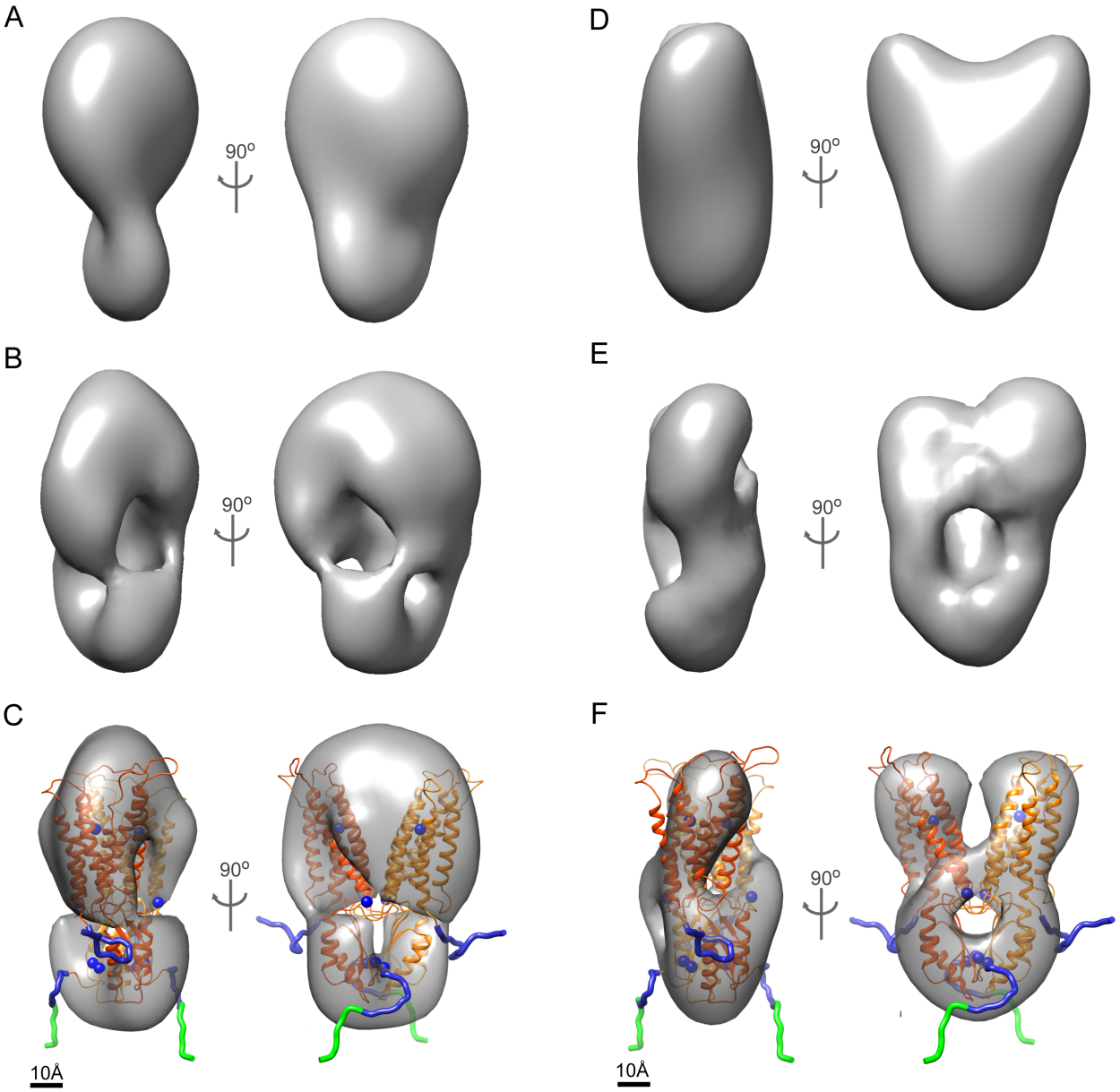

Figure S9. Steps in the determination of the 3D structure of ZnT8. (A) Reference-free EMAN2 reconstruction of ZnT8, without symmetry, at 50 Å resolution. (B) Reconstruction of ZnT8, without symmetry, at 20 Å resolution, generated by RELION using the map of panel A as a reference. (C) Reconstruction of ZnT8, with C2 symmetry applied, at 20 Å resolution, generated by RELION using map of panel A as a reference. (D) Map of YiiP derived from the X-ray structure (PDB ID 3H90) filtered to 50 Å resolution. (E) Reconstruction of ZnT8, without symmetry, at 20 Å resolution, generated by RELION using the map of YiiP in panel D as a reference. (F) Final reconstruction of ZnT8, with C2 symmetry applied, at 20 Å resolution, generated by RELION using YiiP map of panel D as a reference. The isosurface was set at the

volume of a ZnT8 dimer, based on a protein partial specific volume of 0.74 cm^3/g. For the single-particle analyses shown in panels B, C, E, and F, 23 2D class averages were derived from ~3,500 particles. A homology model of ZnT8 based on the X-ray structure of YiiP is docked within the molecular boundary of ZnT8 in panels C and F. Subunits (orange and yellow), zinc ions (blue spheres), amino-terminal fragment (blue), His_6 tag (green). Scale bar denotes 10 Å.

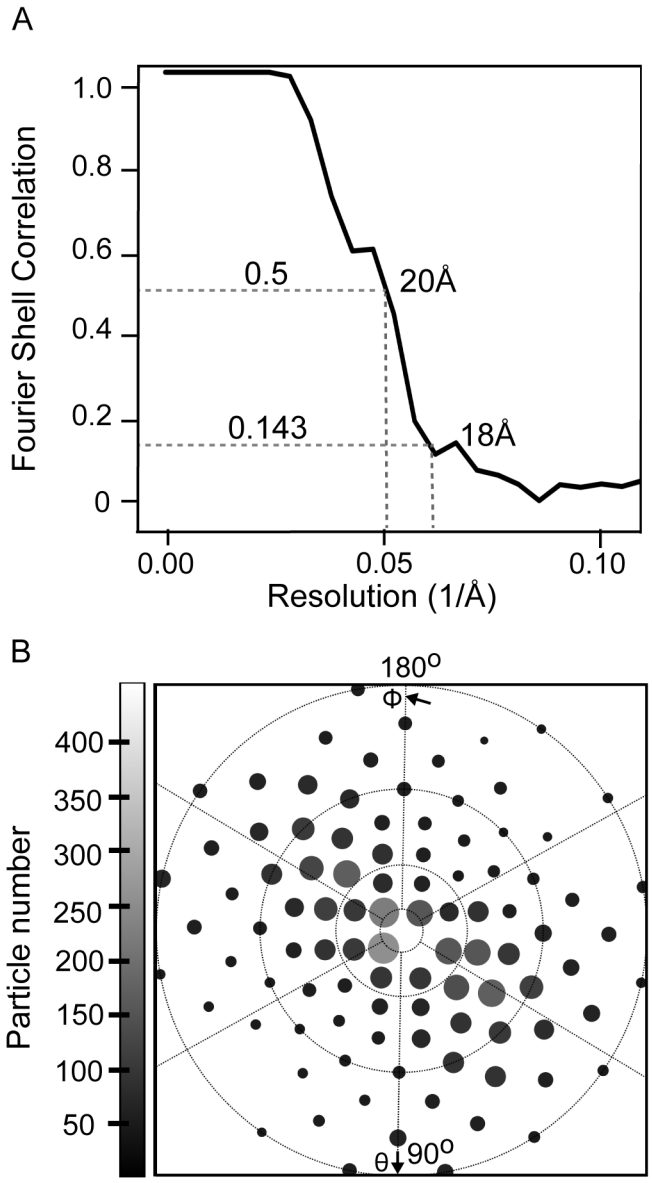

Figure S10. ZnT8B EM reconstruction statistics using a reference-free model. (A) Fourier shell correlation (FSC) between two EM density maps (solid line), each calculated from half of the data. The FSC drops below 0.5 at ~20 Å resolution. (B) Euler angle plot showing angular distribution of particle orientations. Each spot represents a particular orientation of the two Euler angles ϕ (phi) and Θ (theta), and is assigned a size and greyscale value corresponding to the number of particles with that orientation.

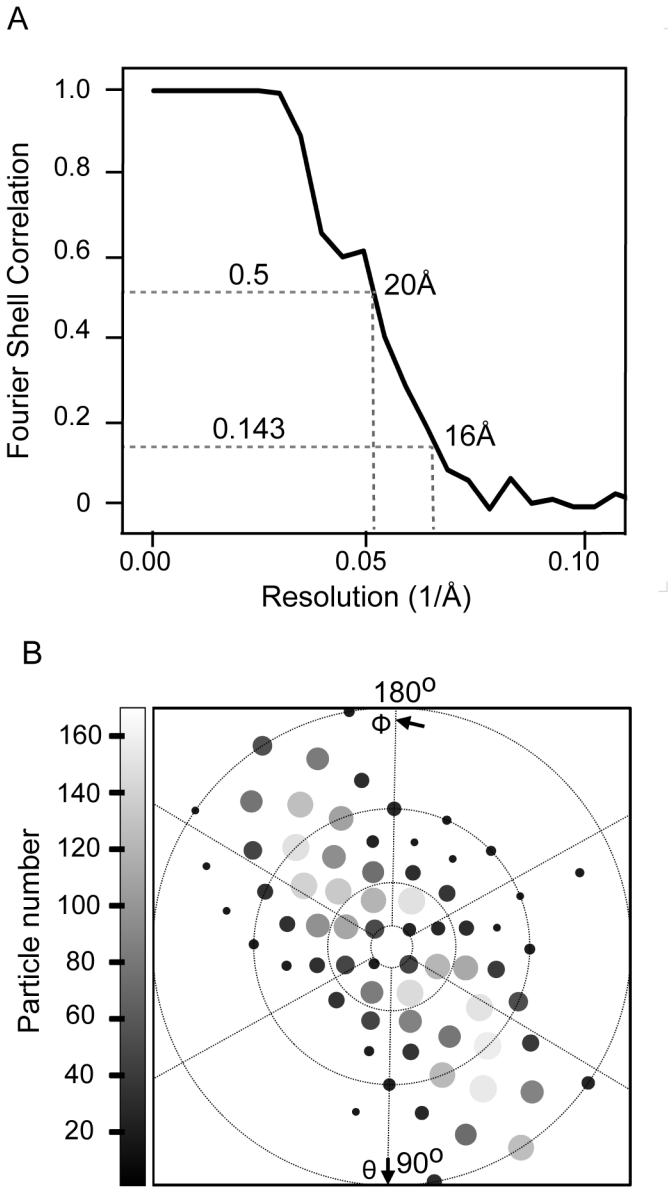

Figure S11. ZnT8B EM reconstruction statistics with YiiP as a starting model. (A) Fourier shell correlation (FSC) between two EM density maps (solid line), each calculated from half of the data. The FSC drops below 0.5 at ~20 Å resolution. (B) Euler angle plot showing angular distribution of particle orientations. Each spot represents a particular orientation of the two Euler angles ϕ (phi) and Θ (theta), and is assigned a size and greyscale value corresponding to the number of particles with that orientation.